Digital Discovery

ROYAL SOCIETY OF CHEMISTRY

PAPER

View Article Online
View Journal | View Issue

Cite this: *Digital Discovery*, 2023, **2**, 1026

A SAR and QSAR study on cyclin dependent kinase 4 inhibitors using machine learning methods†

Xiaoyang Pang,[a] Yunyang Zhao,[a] Guo Li,[a] Jianrong Liu*[b] and Aixia Yan *[a]

Cyclin dependent kinase 4 (CDK4) is a promising target for cancer treatment, and developing new effective CDK4 inhibitors is of great significance in anticancer therapy. In this study, we conducted a structure activity relationship (SAR) study on 3018 CDK4 inhibitors. We applied four machine learning methods, which were Multiple Linear Regression (MLR), Random Forest (RF), Support Vector Machine (SVM) and Deep Neural Network (DNN), to develop 18 classification models based on 3018 inhibitors (dataset 1), 18 classification models based on dataset 1 and decoys, and 24 quantitative structure–activity relationship (QSAR) models based on 1427 inhibitors (dataset 2). We obtained some optimal models. Based on dataset 1, Model A2, built by SVM and MACCS fingerprints, has a prediction accuracy (*Q*) of 92.68% and a Matthews correlation coefficient (MCC) of 0.874 for the test set. Based on dataset 1 and decoys, Model C2, built by SVM and MACCS fingerprints, has a *Q* of 98.5% and a MCC of 0.937 for the test set. Based on dataset 2, Model F7, built by SVM and MOE descriptors, has a coefficient of determination (R^2) of 0.824 and a root mean squared error (RMSE) of 0.534 for the test set. For classification models, it was found that the more samples used for modelling, the more robust the models, and the better the performance of the models. Moreover, we clustered 3018 inhibitors into 12 subsets, and analysed their scaffolds and fragment features. It was found that 2-aminopyrimidine, pyridine, piperazine and cyclopentane were common scaffolds and fragments in highly active inhibitors. This study can provide guidance for the discovery and optimization of CDK4 inhibitor lead compounds.

Received 18th December 2022
Accepted 29th May 2023

DOI: 10.1039/d2dd00143h

rsc.li/digitaldiscovery

Introduction

Cyclin dependent kinase 4 (CDK4) (EC 2.7.11.22), a member of the cyclin dependent kinases family, which belongs to serine/threonine protein kinases,[1] plays an essential role in cell cycle regulation. CDK4 is important in the cell cycle transition from the G1 phase to S phase,[2] binding to cyclin D, after which it phosphorylates and inhibits retinoblastoma (RB) family proteins, and hyper-phosphorylated RB releases E2F, activating a transcriptional program that initiates the S phase.[3] In many cancers, CDK4 is hyper-activated, thereby driving uncontrolled cell proliferation.[4] Hyper-activation of CDK4 is reported in breast cancer, non-small cell lung cancer, melanoma, and endometrial cancer.[5] Therefore, CDK4 is an important antitumor target.

There are five drugs that have been launched so far that target CDK4, namely palbociclib,[6] ribociclib,[7] abemaciclib,[8] trilaciclib[9] and dalpiciclib.[10] Their structures and activities are shown in Table 1, and they are used to treat breast cancer[11–15] and extensive-stage small cell lung cancer.[16] But nowadays there are breast cancer patients resistant to CDK4 inhibitors and endocrine therapy in the clinic.[17–20] Therefore, it is necessary to develop new CDK4 inhibitors.

Computer-aided drug design (CADD) as a convenient and low-cost approach[21] is used to discover CDK4 inhibitor lead compounds. As a method of CADD, a classification model[22–26] is used for structure–activity relationship research and virtual screening of inhibitors, and a QSAR model[27–39] is used to predict the inhibitory activity of a compound. Wu *et al.*[22] built classification models and QSAR models to study the structure–activity relationship of tyrosinase inhibitors. Huo *et al.*[26] built classification models and QSAR models of EGFR inhibitors, and used them for virtual screening. 18 novel EGFR inhibitors were predicted to be highly active, and nine of the 18 novel EGFR inhibitors have been proved to be effective by experiments. As for the study of CDK4 inhibitors, Omar Husham Ahmed *et al.*[39] designed 52 pyrido[2,3-*d*]pyrimidin-7-one-based CDK4 inhibitors, and then developed 2D- ($R^2 = 0.6974$, RMSE = 0.7193) and 3D-quantitative structure–activity relationship (QSAR) models ($R^2 = 0.7649$, RMSE = 0.5809). Virtual screening of the ChEMBL database was carried out using the validated QSAR model and the molecular docking procedure. A total of six compounds were identified as potentially novel CDK4 inhibitor lead compounds. Le *et al.*[40] built 3D-QSAR models with comparative molecular field analysis

[a]*State Key Laboratory of Chemical Resource Engineering, Department of Pharmaceutical Engineering, Beijing University of Chemical Technology, Beijing, P. R. China. E-mail: yanax@mail.buct.edu.cn*

[b]*BUCT-Paris Curie Engineer School, Beijing University of Chemical Technology, Beijing 100029, P. R. China. E-mail: liujianrong2017@126.com*

† Electronic supplementary information (ESI) available. See DOI: https://doi.org/10.1039/d2dd00143h

Table 1 Launched drugs as CDK4 inhibitors

Drug	Structure	IC_{50}
Palbociclib	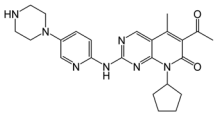	11 nM
Ribociclib	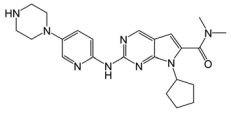	10 nM
Abemaciclib	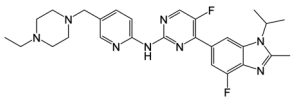	2 nM
Trilaciclib	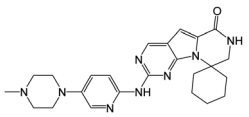	0.4 nM
Dalpiciclib	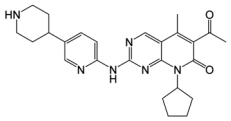	12 nM

(CoMFA) (CDK4: $Q^2 = 0.543$, $R^2 = 0.967$; CDK6: $Q^2 = 0.624$, $R^2 = 0.984$) and comparative molecular similarity indices analysis (CoMSIA) (CDK4: $Q^2 = 0.518$, $R^2 = 0.937$; CDK6: $Q^2 = 0.584$, $R^2 = 0.975$) based on 52 dual CDK4/6 inhibitors, and then designed 10 novel compounds with expected activity and ADME/T properties. Sarhan *et al.*[38] synthesized novel 6-bromo-coumarin-ethylidene-hydrazonyl-thiazolyl and 6-bromo-coumarin-thiazolyl based derivatives, and built a QSAR model (R^2 = 0.92, RMSE = 0.44) based on 16 previously reported thiazolyl-hydrazono-coumarin compounds. Five compounds predicted by the QSAR model were verified to have potential anticancer activities, and one of them was considered as a selective radiotherapy agent for solid tumours with promising anticancer activity based on the results of experiments *in vitro*. Therefore, the classification model and QSAR model are helpful for the discovery and optimization of CDK4 inhibitors.

The previous studies on CDK4 inhibitors were carried out based on a certain scaffold, so it is not easy to find novel scaffolds of inhibitors. To address this issue, in this work, 3018 CDK4 inhibitors were collected to research the structure–activity relationship in this study. We calculated MACCS fingerprints, ECFP4 fingerprints and Corina descriptors, using Random Forest, Support Vector Machine and Deep Neural Network methods to build classification models, to distinguish highly/weakly active inhibitors. Then we calculated Corina, MOE and RDKit descriptors, using Multiple Linear Regression, Random Forest, Support Vector Machine and Deep Neural Network methods to build QSAR models, to predict the CDK4 inhibitory activity of the compound. In addition, we clustered 3018 CDK4 inhibitors to 12 subsets and analysed the features of the scaffolds and fragments. This work aims to study the relationship between the structures and activities of CDK4 inhibitors, and investigate the scaffolds and fragment features of highly active CDK4 inhibitors.

Materials and methods

Dataset

For classification models, a total of 3018 CDK4 inhibitors and their IC_{50} were collected from 250 pieces of literature (access date: 2022.8) as dataset 1, with IC_{50} ranging from 0.13 nM to 1000 μM.

We selected 200 nM as a threshold to distinguish highly and weakly active inhibitors. If the IC_{50} of one compound is less than 200 nM, it is defined as a highly active inhibitor with a label of 1; in contrast, if the IC_{50} of one compound is more than 200 nM, it is defined as a weakly active inhibitor with a label of 0. As a result, 1642 compounds were distinguished as highly active inhibitors, and 1376 compounds were distinguished as weakly active inhibitors. We divided dataset 1 into training set 1 (2266 inhibitors) and test set 1 (752 inhibitors) by a Self-Organizing Map (SOM)[41] and divided dataset 1 into training set 2 (2263 inhibitors) and test set 2 (755 inhibitors) by a random method. SOM is performed by SONNIA software[42] and MACCS fingerprints of compounds, and it enables the chemical space of the training set to cover that of the entire dataset as much as possible. The training set divided by SOM can have rich chemical structure diversity.

In addition, because it is well known that decoys are necessary to evaluate virtual screening methods,[43] we also added decoys into dataset 1 to build classification models. To avoid decoy bias, we used two different decoy generation methods for the training set and test set, respectively.[44]

We used Deepcoy[45] to generate decoys based on the training set. Training set 1 contains 2266 inhibitors, 1204 of which are highly active, and based on these highly active inhibitors, we generated 5951 decoys, training set 1 and these decoys form training set 3, which includes 8217 molecules. Training set 2 contains 2263 inhibitors, 1231 of which are highly active, and based on these highly active inhibitors, we generated 6085 decoys, training set 2 and these decoys form training set 4, which includes 8348 molecules. We used MUBD-DecoyMaker2.0 [46] to generate decoys based on the test set. Test set 1 contains 752 inhibitors, 438 of which are highly active, and based on these highly active inhibitors, we generated 2377 decoys, test set 1 and these decoys form test set 3, which includes 3129 molecules. Test set 2 contains 755 inhibitors, 411 of which are highly active, and based on these highly active inhibitors, we generated 2379 decoys, test set 2 and these decoys form test set 4, which includes 3134 molecules.

For QSAR models, based on dataset 1, 1427 compounds whose IC_{50} was detected by a radiolabeling method were selected as dataset 2, with IC_{50} ranging from 0.13 nM to 1000 μM. Before modelling, we need to convert IC_{50} into pIC_{50} ($pIC_{50} = \log(IC_{50})$, in the unit of mol L^{-1}), to eliminate the influence of magnitudes. pIC_{50} ranges from 3 to 9.89. We divided dataset 2 into training set 5 and test set 5 by SOM, and divided dataset 2 into training set 6 and test set 6 by a random method.

Generated decoys evaluation

The optimal embedding score (DOE score) and doppelganger score were used to evaluate generated decoys.[45] The DOE score measures the quality of the embedding of actives and decoys in chemical space. An optimal embedding of actives and decoys achieves a DOE score of zero, while complete separation in physicochemical space results in a DOE score of 0.5. The average doppelganger score is a measure of the structural similarity between actives and decoys, when the value is less than 0.4, indicating that the generated decoys have an allowable false negative bias.

Calculation and extraction of descriptors

For classification models, we calculated three types of descriptors for modelling, MACCS fingerprints,[47] ECFP4 fingerprints[48] and Corina descriptors.[49] MACCS fingerprints have 166 bits, and ECFP4 fingerprints have 1024 bits, and both of them are calculated by the RDkit v2020.09.1 package.[50] The Corina descriptors consist of 108 descriptors calculated by CORINA Symphony software.[49]

The extraction of descriptors is based on the training set. As for MACCS and ECFP4 fingerprints, we calculated the variance of each bit, and extracted the bits whose variance is larger than the mean variance. As for Corina descriptors, we calculated the Pearson coefficient[51] between descriptors and activity, and then extracted the descriptors whose coefficient with activity is larger than 0.1, then when the coefficient between the two descriptors is larger than 0.9, we extracted the descriptor whose coefficient with activity is larger than another. As a result, we got a set of Corina descriptors for modelling. Before modelling, the selected Corina descriptors' values were scaled to [0.1, 0.9] using eqn (1):

$$X_i^* = \frac{X_i - X_{\min}}{X_{\max} - X_{\min}} \times 0.8 + 0.1 \quad (1)$$

where X_i^* is the scaled value, X_i is the original value, and $X_{\min}$ and $X_{\max}$ represent the minimum and maximum values in the training set, respectively.

For classification models based on dataset 1 and decoys, we also calculated MACCS fingerprints, ECFP4 fingerprints and Corina descriptors. Based on the training set, as for MACCS and ECFP4 fingerprints, we calculated the variance of each bit to extract descriptors, and as for Corina descriptors, we calculated the Pearson coefficient between descriptors and activity to extract descriptors. Before modelling, the extracted Corina descriptors' values were scaled to [0.1, 0.9] using eqn (1).

For QSAR models, we calculated three types of descriptors for modelling, Corina descriptors, MOE descriptors[52] and RDkit descriptors.[50] The MOE descriptors consist of 206 descriptors calculated by MOE software.[52] The RDkit descriptors consist of 208 descriptors calculated by the RDkit v2020.09.1 package.[50] Based on the training set, we calculated the Pearson coefficient[51] between descriptors and activity to extract descriptors, and then scaled the extracted descriptors using eqn (1) to build QSAR models.

Modelling methods

For classification models, we used Random Forest (RF),[53] Support Vector Machine (SVM)[54] and Deep Neural Network (DNN)[55] methods to build models. Random Forest[53] is an ensemble algorithm that scores based on the results of multiple decision trees. Support Vector Machine[54] distinguishes samples by mapping them to a higher dimensional space. The Scikit-learn v1.0.2 package[56] was used to build RF models and SVM models, and Grid Search[57] which is based on the 5-fold cross-validation accuracy[58] and repeated training[59] was used to find the optimal parameters. In this study, DNN models have three hidden layers, and a batch normalization layer[60] was added after each layer to prevent model overfitting. The optimization algorithm used was Adam.[61] We took the 5-fold cross-validation and repeated training strategy[59] to train the DNN models, and adopted early-stopping function[62] to stop training, when the binary cross entropy on the validation set is not improved in 30 consecutive epochs. The Pytorch v1.10.0 package[63] was used to build DNN models.

For QSAR models, we used Multiple Linear Regression (MLR),[64] Random Forest (RF),[53] Support Vector Machine (SVM)[54] and Deep Neural Network (DNN)[55] methods to build models. Multiple Linear Regression[64] belongs to linear regression and has poor fitting for nonlinear problems. Both Random Forest[53] and Support Vector Machine[54] can be used to solve classification and regression problems. As for the early-stopping function of DNN models, the evaluation parameter is mean squared error (MSE).[65] The training strategy of QSAR models is the same as that of the classification models. The Scikit-learn v1.0.2 package[56] was used to build MLR, RF and SVM models, while the Pytorch v1.10.0 package[63] was used to build DNN models.

Model evaluation

For classification models, the accuracy (Q), sensitivity (SE),[66] specificity (SP)[66] and Matthews correlation coefficient (MCC)[67] of the training and testing sets were used to evaluate performance. The cross-validation of 5-fold (5-CV)[58] on the training set was used to evaluate the robustness of the model.

For QSAR models, the coefficient of determination (R^2),[68] mean absolute error (MAE)[65] and root mean squared error (RMSE)[65] were used to evaluate performance.

Applicability domain

For classification models, $d_{\text{STD-PRO}}$,[69] the predictive reliability of compounds was used to define the application domain of the model. $D_{\text{STD-PRO}}$ can be calculated based on the prediction probability of all models, and compound J's $d_{\text{STD-PRO}}$ can be calculated using eqn (2).

$$d_{\text{STD-PRO}} = \min\left\{ \begin{array}{l} \int_{0.5}^{+\infty} N(x, y(J), \sigma(J))\mathrm{d}x \\ \int_{-\infty}^{0.5} N(x, y(J), \sigma(J))\mathrm{d}x \end{array} \right\} \quad (2)$$

where $y(J)$ and $\sigma(J)$ are the average and standard deviation of probability of compound J predicted by the N model,

respectively. $N(x)$, $y(J)$, $\sigma(J)$ are the normal distribution density function of probability. We selected one of the compounds' $d_{\text{STD-PRO}}$ in the training set as the applicability domain (AD) threshold of a model, and compounds whose $d_{\text{STD-PRO}}$ is less than the threshold are considered to be within the applicability domain of the model.

For QSAR models, the Williams plot[70] is used to visualize the application domain of the model. In the Williams plot, the standardized residuals (σ) and leverage (h) values of the compounds are calculated to determine whether they are in the application domain of the model. The σ value is the difference between the true value and predicted value. The h value of a compound can be calculated using eqn (3). When the leverage value of a compound is less than the leverage warning value (h^*), it is in the application domain. The h^* value can be calculated using eqn (4).

$$h_i = x_i^T (X^T X)^{-1} x_i \quad (3)$$

$$h^* = 3(p + 1)/n \quad (4)$$

where x_i is the vector of descriptors for the ith compound and X is the descriptor matrix of the training set, while p is the number of descriptors used in the model and n is the number of molecules in the training set.

Clustering methods

We used two clustering methods to cluster inhibitors, which are K-means[71] and hierarchical clustering (HC).[72] In addition, we used two dimension-reduction methods to reduce the high dimensions data to two-dimensions, which are t-Distributed Stochastic Neighbour Embedding (TSNE)[73] and Uniform Manifold Approximation and Projection (UMAP).[72] K-Means[71] belongs to unsupervised machine learning. It achieves the effect of clustering by constantly taking the samples closest to the mean of seed points to aggregate data. HC[72] consists in building a binary merge tree, starting from the molecules stored at the leaves and merging them until reaching the root of the tree that contains all the molecules of the dataset. TSNE[73] is an embedding model that can map data from a high-dimensional space to a low-dimensional space and retain the local characteristics of the data. UMAP[72] is a non-linear dimensionality reduction algorithm that seeks to learn the manifold structure of the data and find a low-dimensional embedding while preserving the essential topological structure of that manifold. K-Means, HC, TSNE and UMAP are implemented by the Scikit-learn v1.0.2 package.[56]

Clustering evaluation

To measure the quality of clustering, we considered three unsupervised metrics to evaluate the clustering quality results, the silhouette coefficient, the Calinski–Harabasz (CH) score, and the Davies–Bouldin (DB) score.[72] As for the silhouette coefficient, the best value is 1, and the worst value is −1; negative values generally indicate that a molecule has been assigned to the wrong cluster as a different cluster is more similar. As for the CH score, a higher value relates to a model with better-defined clusters. As for the DB score, the minimum score is zero, with lower values indicating better clustering. These metrics are implemented by the Scikit-learn v1.0.2 package.

Statistical methods for analysing fragments

We used the BRICS function in the RDkit v2020.09.1 package[50] to split molecular structures into a set of fragments, and then counted the frequencies of each fragment in highly and weakly active inhibitors respectively to analyse fragment features. When the proportion of highly/weakly active inhibitors in the subset was less than 10%, these compounds were considered not statistically significant and were not counted.

Results and discussion

Classification models (based on dataset 1)

For training set 1 (divided by SOM), we calculated and extracted three types of descriptors (76 MACCS fingerprints, 294 ECFP4 fingerprints, and 24 Corina descriptors), using three machine learning methods (RF, SVM and DNN) to build Models A1–A9. For training set 2 (divided by a random method), we calculated and extracted three types of descriptors (76 MACCS fingerprints, 293 ECFP4 fingerprints, and 24 Corina descriptors), using three machine learning methods (RF, SVM and DNN) to build Models B1–B9. The performances of the 18 classification models are shown in Table 2. The optimal hyper-parameters of each model are given in the ESI.†

According to Table 2, it was found that the differences between SE and SP of all models are very small, indicating that all models can balance different types of inhibitors very well. The 5-CV accuracies of all models are greater than 82%, indicating that all models are robust. The MCC values on the test set of all models are greater than 0.77, indicating that all models have good performance. The prediction accuracies on the training set and test set of all models are more than 85%, indicating that all models have good performance of fitting and prediction respectively.

Comparing the performances of models built by different methods, it was found that the models built by SVM have the best performance on the test set, and the models built by DNN have the best robustness. Comparing the performances of models based on different descriptors, it was found that the models based on ECFP4 fingerprints have the best performance on the test set. The models based on Corina descriptors have good performance with a small number of descriptors, indicating that the extracted Corina descriptors are very important for inhibitory activity.

Comparing the performances of models based on the two different training sets, the optimal models were selected according to the prediction MCC on the test set. It was found that among Models A1–A9 based on training set 1 (divided by SOM), Model A2 is the optimal model, which is built by MACCS fingerprints and SVM, and the prediction accuracy on the test set is 93.88%, and MCC is 0.874. Among Models B1–B9 based on training set 2 (divided by a random method), Model B5 is the optimal model, which is built by ECFP4 fingerprints and SVM, and the prediction accuracy on the test set is 89.93%, and MCC

Table 2 Performances of the 18 classification models (based on dataset 1)

Model	Training set/test set	Input descriptors		Methods	Training set			Test set			
		Type	n^a		Q^b (%)	5-CV^c (%)	MCC^d	Q (%)	SE^e (%)	SP^f(%)	MCC
Model A1	2266/752	MACCS	76	RF	85.79	82.44	0.715	90.03	90.41	89.49	0.796
Model A2	2266/752	MACCS	76	SVM	89.36	83.85	0.787	93.88	94.75	92.68	0.874
Model A3	2266/752	MACCS	76	DNN	87.03	85.99	0.739	90.43	89.04	92.36	0.807
Model A4	2266/752	ECFP4	294	RF	87.29	84.91	0.745	91.49	89.95	93.63	0.829
Model A5	2266/752	ECFP4	294	SVM	91.92	86.23	0.838	93.62	93.38	93.95	0.870
Model A6	2266/752	ECFP4	294	DNN	87.95	86.96	0.759	90.56	88.58	93.31	0.811
Model A7	2266/752	Corina	24	RF	89.23	83.62	0.784	91.20	89.93	92.97	0.822
Model A8	2266/752	Corina	24	SVM	89.32	84.64	0.785	92.27	91.30	93.61	0.843
Model A9	2266/752	Corina	24	DNN	86.14	85.12	0.722	90.13	89.24	91.37	0.800
Model B1	2263/755	MACCS	76	RF	86.92	84.58	0.736	87.15	87.83	86.34	0.741
Model B2	2263/755	MACCS	76	SVM	91.21	86.30	0.823	88.48	90.27	86.34	0.768
Model B3	2263/755	MACCS	76	DNN	89.35	88.30	0.786	86.89	89.78	83.43	0.735
Model B4	2263/755	ECFP4	293	RF	88.73	86.39	0.773	88.61	87.59	89.83	0.772
Model B5	2263/755	ECFP4	293	SVM	93.28	87.58	0.865	89.93	90.02	89.83	0.798
Model B6	2263/755	ECFP4	293	DNN	90.01	89.49	0.800	86.62	89.78	82.85	0.730
Model B7	2263/755	Corina	24	RF	90.53	86.02	0.809	85.70	85.89	85.47	0.712
Model B8	2263/755	Corina	24	SVM	93.01	87.08	0.859	86.49	86.62	86.34	0.728
Model B9	2263/755	Corina	24	DNN	86.95	86.68	0.738	87.02	89.78	83.72	0.738

[a] n, number of descriptors. [b] Q, accuracy. [c] 5-CV, 5-fold cross-validation. [d] MCC, Matthews correlation coefficient. [e] SE, sensitivity. [f] SP, specificity.

is 0.798. The two optimal models are both SVM models, indicating that SVM is a suitable method for this study.

Application domain of classification models

Based on the 18 classification models, we calculated the $d_{\text{STD-PRO}}$[69] of each compound. As for the training set, the prediction probabilities of the models were replaced by the 5-CV probabilities. When the 5-CV accuracy of the model is 90%, the model is considered reliable. Therefore, we selected the threshold to make the 5-CV accuracy exactly 90% ($\text{Threshold}_{0.90}$). Table 3 shows the threshold, and the coverage and performances on the training set and test set within application domain.

According to Table 3, we found that within application domain, the prediction accuracy and MCC on the test set are

Table 3 The application domain of the 18 classification models

Model	$\text{Threshold}_{0.90}$[a]	Training set			Test set		
		Coverage[b](%)	5-CV^c (%)	MCC^d	Coverage (%)	Q^e (%)	MCC
Model A1	0.107	81.95	90.03	0.799	87.20	94.95	0.897
Model A2	0.114	82.66	90.01	0.798	87.60	96.35	0.925
Model A3	0.108	82.08	90.05	0.799	87.33	96.03	0.919
Model A4	0.131	83.98	90.01	0.799	88.40	95.93	0.917
Model A5	0.096	80.76	90.05	0.799	86.40	95.83	0.915
Model A6	0.107	81.95	90.03	0.799	87.20	96.33	0.925
Model A7	0.086	79.79	90.04	0.799	86.00	95.50	0.909
Model A8	0.089	80.23	90.04	0.799	86.27	94.28	0.884
Model A9	0.083	79.35	90.04	0.799	85.73	95.96	0.917
Model B1	0.176	87.04	90.04	0.798	90.07	91.03	0.819
Model B2	0.231	90.40	90.01	0.798	92.19	90.66	0.812
Model B3	0.222	89.87	90.00	0.798	92.05	90.94	0.817
Model B4	0.223	90.05	90.02	0.798	92.05	91.80	0.835
Model B5	0.186	87.48	90.04	0.798	90.46	90.34	0.806
Model B6	0.176	86.91	90.02	0.798	89.93	89.69	0.793
Model B7	0.154	85.71	90.04	0.798	88.87	90.46	0.807
Model B8	0.198	88.41	90.04	0.798	91.13	89.83	0.794
Model B9	0.191	87.75	90.02	0.799	90.73	90.95	0.817

[a] $\text{Threshold}_{0.90}$, the threshold of the model when the accumulative accuracy of 5-fold cross-validation is close to 90%. [b] Coverage, the proportion of compounds corresponding to $\text{Threshold}_{0.90}$. [c] 5-CV, 5-fold cross-validation. [d] MCC, Matthews correlation coefficient. [e] Q, accuracy

improved. The threshold of Models A1–A9 ranges from 0.08 to 0.13, and the coverage of the training set and test set ranges from 80% to 87%, respectively. The threshold of Models B1–B9 ranges from 0.15 to 0.23, and the coverage of the training set and test set ranges from 87% to 90%, respectively. According to the MCC on the test set, Model A2 was the optimal model. Model A2 is the model built by MACCS fingerprints and SVM, with the threshold of 0.114. The coverage of the training set and test set is 82.66% and 87.6%, respectively, and the prediction accuracy on the test set is 96.35% and MCC is 0.925.

Classification models (based on dataset 1 and decoys)

Firstly, we measured the quality of generated decoys. The evaluation of generated decoys is shown in Table S1 in the ESI.† According to Table S1,† it was found that the DOE score between the training set/test set and generated decoys is less than 0.1, indicating that the quality of the embedding of actives and decoys in chemical space is good, and the average doppelganger score between training set/test set and generated decoys is less than 0.25, indicating that the structural similarity between actives and decoys is low, and the generated decoys have a good false negative bias, and the quality of generated decoys is good.

For training set 3, we calculated and extracted three types of descriptors (81 MACCS fingerprints, 299 ECFP4 fingerprints, and 13 Corina descriptors), using three machine learning methods (RF, SVM and DNN) to build Models C1–C9. For training set 4, we calculated and extracted three types of descriptors (81 MACCS fingerprints, 298 ECFP4 fingerprints, and 16 Corina descriptors), using three machine learning methods (RF, SVM and DNN) to build Models D1–D9. The performances of the 18 classification models are shown in Table 4. The optimal hyper-parameters of each model are given in the ESI.†

According to Table 4, we found that the differences between SE and SP of most models are within the permissible limits, especially the models based on training set 3, indicating that the models can balance different types of inhibitors very well. The 5-CV accuracies of all models are greater than 90%, indicating that all models are robust. The MCC values on the test set of all models are greater than 0.74, indicating that all models have good performance. The prediction accuracies on the training set and test set of all models are more than 93%, indicating that all models have good performance of fitting and prediction respectively.

Compared to the models without decoys (Models A1–A9 and B1–B9 in Table 2), the 5-CV accuracies, average MCC and prediction accuracies for the training set and test set get better, indicating that the more samples used for modelling, the more robust the models, and the better the performance of the models.

While the differences between SE and SP increased to some extent, the reason for which is that the number of weakly active inhibitors has increased significantly, the different types of inhibitors used for modelling are unevenly distributed.

Comparing the performances of models built by different methods, it was found that the models built by SVM and RF have better performance on the test set than other models. Comparing the performances of models based on different descriptors, it was found that the models based on ECFP4 fingerprints have the best performance on the test set.

Comparing the performances of models based on the two different training sets, the optimal models were selected according to the prediction MCC on the test set. It was found that among Models C1–C9 based on training set 3, Model C2 is the optimal model, which is built by MACCS fingerprints and SVM, and the prediction accuracy on the test set is 98.5%, while MCC is 0.937. Among Models D1–D9 based on training set 4,

Table 4 Performances of the 18 classification models (based on dataset 1 and decoys)

Model	Training set/test set	Input descriptors		Methods	Training set			Test set			
		Type	*n*		*Q* (%)	5-CV (%)	MCC	*Q* (%)	SE (%)	SP (%)	MCC
Model C1	8217/3129	MACCS	81	RF	98.93	93.90	0.957	98.40	92.91	99.29	0.933
Model C2	8217/3129	MACCS	81	SVM	98.54	93.89	0.942	98.50	92.22	99.52	0.937
Model C3	8217/3129	MACCS	81	DNN	98.78	95.64	0.951	96.52	88.79	97.77	0.857
Model C4	8217/3129	ECFP4	299	RF	99.99	95.85	1.000	97.67	92.22	98.55	0.903
Model C5	8217/3129	ECFP4	299	SVM	99.94	95.61	0.998	98.34	93.14	99.18	0.930
Model C6	8217/3129	ECFP4	299	DNN	98.47	90.96	0.938	96.74	85.81	98.51	0.862
Model C7	8217/3129	Corina	13	RF	99.60	93.55	0.984	97.12	82.61	99.48	0.876
Model C8	8217/3129	Corina	13	SVM	96.73	94.39	0.868	96.71	86.27	98.40	0.861
Model C9	8217/3129	Corina	13	DNN	94.01	93.24	0.750	94.95	76.20	97.99	0.781
Model D1	8348/3134	MACCS	81	RF	99.09	95.29	0.964	96.49	82.97	98.53	0.842
Model D2	8348/3134	MACCS	81	SVM	96.61	95.27	0.863	96.49	82.48	98.60	0.841
Model D3	8348/3134	MACCS	81	DNN	98.97	97.22	0.959	93.94	79.81	96.07	0.741
Model D4	8348/3134	ECFP4	298	RF	99.99	96.31	1.000	97.19	86.37	98.82	0.874
Model D5	8348/3134	ECFP4	298	SVM	97.07	96.24	0.884	97.32	88.81	98.60	0.881
Model D6	8348/3134	ECFP4	298	DNN	98.51	91.81	0.940	96.20	80.78	98.53	0.828
Model D7	8348/3134	Corina	16	RF	99.69	94.85	0.988	95.88	75.67	98.93	0.810
Model D8	8348/3134	Corina	16	SVM	96.62	95.40	0.863	95.98	82.73	97.98	0.821
Model D9	8348/3134	Corina	16	DNN	94.69	93.33	0.782	94.54	73.72	97.69	0.751

Model D5 is the optimal model, which is built by ECFP4 fingerprints and SVM, and the prediction accuracy on test set 4 is 87.32%, while MCC is 0.881.

QSAR models

For training set 5 (divided by SOM), we calculated and extracted three types of descriptors (24 Corina descriptors, 33 MOE descriptors, and 31 RDkit descriptors), using four machine learning methods (MLR, RF, SVM and DNN) to build Models E1–E12. For training set 6 (divided by a random method), we calculated and extracted three types of descriptors (27 Corina descriptors, 43 MOE descriptors, and 45 RDkit descriptors), using four machine learning methods (MLR, RF, SVM and DNN) to build Models F1–F12. The performances of the 24 QSAR models are shown in Table 5. The optimal hyper-parameters of each model are given in the ESI.†

We selected R^2 as the most important evaluation standard, and found that except for the multiple linear regression models, the prediction R^2 of the other 18 models on the test set was greater than 0.74, indicating that the 18 QSAR models have good performances. The range of RMSE on the test set is 0.534–0.644, and the range of MAE is 0.404–0.579, that means the prediction error is within the acceptable range.

Comparing the performances of models built by different methods, it was found that the models built by SVM have the best performance on the test set, indicating that SVM is the best method for building QSAR models. Comparing the performances of models based on different descriptors, it was found that the models built by MOE descriptors have the best performance on the test set, indicating that the extracted MOE descriptors are very important for inhibitory activity.

Comparing the performances of models based on the two different training sets, the optimal models were selected according to the prediction R^2 on the test set. It was found that among Models E1–E12 based on training set 5 (divided by SOM), Model E3 is the optimal model, which is built by Corina descriptors and SVM, and the prediction R^2 on the test set is 0.805, and RMSE is 0.561. Among Models F1–F12 based on training set 6 (divided by a random method), Model F7 is the optimal model, which is built by MOE descriptors and SVM, and the prediction R^2 on the test set is 0.824, and RMSE is 0.534. Furthermore, we draw the prediction results of Model E3 and Model F7, as shown in Fig. 1.

Application domain of QSAR models

The application domain of QSAR models is visualized by the Williams plot,[70] and the Williams plots of Model E3 and Model F7 are shown in Fig. 2. The points in the left region surrounded by three dashed lines are all inhibitors in the application domain of the model. According to statistics, the coverages of the training set and test set are 97.64% and 95.63% for Model E3, respectively, and they are 98.50% and 99.94% for Model F7, respectively.

Table 5 Performances of the 24 QSAR models

Model	Training set/test set	Input descriptors		Methods	Training set			Test set		
		Type	n^a		R^{2b}	MAE^c	RMSE^d	R^2	MAE	RMSE
Model E1	1061/366	Corina	24	MLR	0.621	0.605	0.764	0.588	0.647	0.816
Model E2	1061/366	Corina	24	RF	0.901	0.311	0.390	0.774	0.453	0.605
Model E3	1061/366	Corina	24	SVM	0.920	0.279	0.351	0.805	0.421	0.561
Model E4	1061/366	Corina	24	DNN	0.886	0.330	0.418	0.778	0.460	0.598
Model E5	1061/366	MOE	33	MLR	0.689	0.547	0.692	0.650	0.595	0.752
Model E6	1061/366	MOE	33	RF	0.905	0.304	0.383	0.764	0.462	0.617
Model E7	1061/366	MOE	33	SVM	0.927	0.214	0.336	0.793	0.437	0.579
Model E8	1061/366	MOE	33	DNN	0.932	0.250	0.323	0.789	0.440	0.583
Model E9	1061/366	RDkit	31	MLR	0.671	0.564	0.712	0.660	0.581	0.743
Model E10	1061/366	RDkit	31	RF	0.904	0.306	0.385	0.796	0.432	0.574
Model E11	1061/366	RDkit	31	SVM	0.936	0.217	0.313	0.805	0.410	0.562
Model E12	1061/366	RDkit	31	DNN	0.932	0.250	0.323	0.770	0.460	0.610
Model F1	1050/357	Corina	27	MLR	0.655	0.548	0.729	0.567	0.639	0.838
Model F2	1050/357	Corina	27	RF	0.901	0.311	0.391	0.744	0.462	0.644
Model F3	1050/357	Corina	27	SVM	0.918	0.279	0.356	0.807	0.427	0.559
Model F4	1050/357	Corina	27	DNN	0.916	0.280	0.359	0.791	0.441	0.582
Model F5	1050/357	MOE	43	MLR	0.721	0.512	0.655	0.657	0.578	0.745
Model F6	1050/357	MOE	43	RF	0.908	0.298	0.376	0.763	0.444	0.619
Model F7	1050/357	MOE	43	SVM	0.969	0.160	0.218	0.824	0.404	0.534
Model F8	1050/357	MOE	43	DNN	0.943	0.225	0.296	0.807	0.427	0.559
Model F9	1050/357	RDkit	45	MLR	0.713	0.518	0.665	0.665	0.564	0.737
Model F10	1050/357	RDkit	45	RF	0.910	0.297	0.373	0.784	0.435	0.592
Model F11	1050/357	RDkit	45	SVM	0.939	0.216	0.306	0.790	0.440	0.583
Model F12	1050/357	RDkit	45	DNN	0.939	0.235	0.306	0.774	0.457	0.605

[a] n, number of descriptors. [b] R^2, coefficient of determination. [c] MAE, mean absolute error. [d] RMSE, root mean squared error.

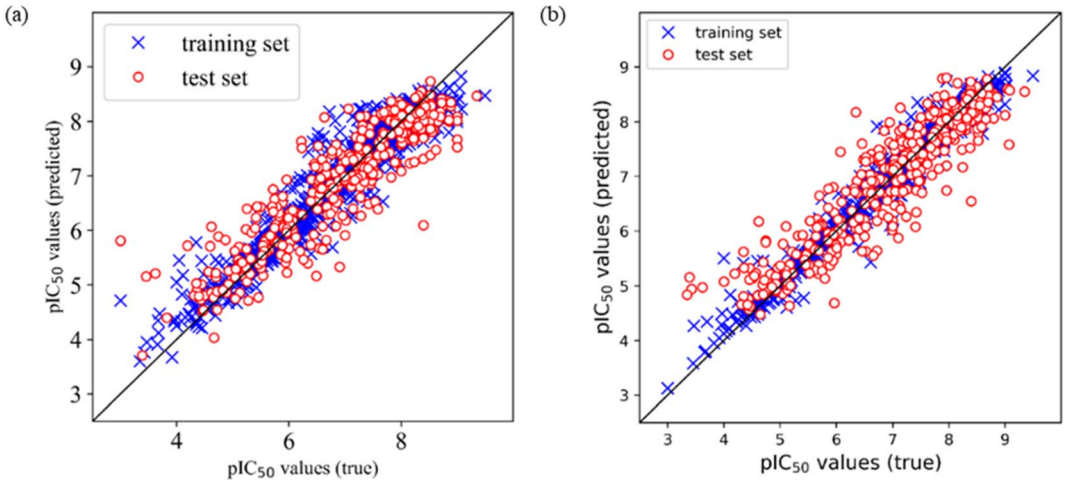

Fig. 1 Predicted *vs.* true (experimental) values of bioactivity (pIC_{50}) of Model E3 and Model F7. (a) The predicted and true bioactivity of Model E3, which is built by Corina descriptors and SVM based on training set 5. (b) The predicted and true bioactivity of Model F7, which is built by MOE descriptors and SVM based on training set 6.

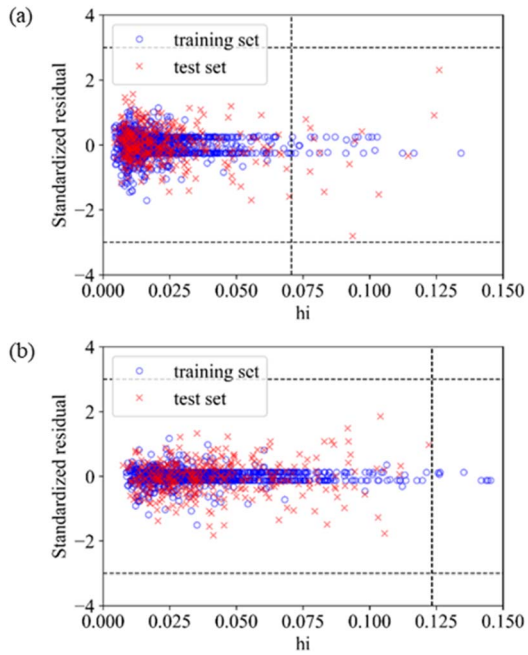

Fig. 2 Application domain of Model E3 and Model F7. (a) The application domain of Model E3, which is built by Corina descriptors and SVM based on training set 5. (b) The application domain of Model F7, which is built by MOE descriptors and SVM based on training set 6.

Table 6 shows the performances of the two optimal models in the application domain. It was found that the RMSE of the two models on the test set shows an improvement, indicating that the application domain can screen out some outliers with large prediction deviation, and the prediction of compounds in the application domain is considered to be reliable.

Clustering results and analysis

In order to study the structure activity relationship of CDK4 inhibitors, we performed clustering, as well as scaffolds and fragment features analysis.

On the basis of dataset 1, we clustered inhibitors based on their ECFP4 fingerprints. The clustering methods are *K*-means and hierarchical clustering, while the dimension-reduction methods are TSNE and UMAP, so we tried two clustering methods and four combinations (TSNE + *K*-means, TSNE + HC, UMAP + *K*-means, and UMAP + HC) which are dimension reduction followed by clustering, so there are 6 different methods. We set the number of categories to 11, and carried out 6 methods to clustering, and then evaluated the results, as shown in Table 7.

According to Table 7, it was found that UMAP + *K*-means has the best performance in the 6 different methods, with the lowest values of silhouette coefficient and DB score, and the highest value of CH score. So, we used this method to explore the appropriate number of categories. We set the number from 9 to 15, and evaluated the clustering results, as shown in Table 8.

Table 6 Performances of Model E3 and Model F7 in the application domain

	Training set			Test set		
Model	R^2	MAE	RMSE	R^2	MAE	RMSE
Model E3	0.920	0.279	0.351	0.805	0.421	0.561
Model E3 (AD)	0.918	0.280	0.354	0.828	0.403	0.519
Model F7	0.969	0.160	0.218	0.824	0.404	0.534
Model F7 (AD)	0.968	0.161	0.219	0.827	0.400	0.528

Table 7 Performance of 6 different clustering methods

Method	Silhouette	CH score	DB score
K-Means	0.13	144.82	2.39
HC	0.13	145.40	2.71
TSNE + *K*-means	0.53	4882.42	0.64
TSNE + HC	0.50	4414.13	0.66
UMAP + *K*-means	0.67	14 780.75	0.45
UMAP + HC	0.64	12 900.34	0.49

Table 8 Performance of UMAP + *K*-means with different number of categories

*n*_cluster[a]	Silhouette	CH score	DB score
9	0.61	11 344.13	0.53
10	0.65	13 013.22	0.45
11	0.67	14 780.75	0.45
12	0.67	16 418.07	0.47
13	0.66	16 410.25	0.49
14	0.64	18 255.97	0.51
15	0.63	18 696.13	0.51

[a] *n*_cluster, the number of categories.

According to Table 8, it was found that when the number is 12, the clustering result has the best silhouette coefficient, good DB score and best CH score. Therefore, we chose 12 as the number of categories.

We clustered 3018 CDK4 inhibitors into 12 subsets by UMAP and *K*-means, and visualized them by the UMAP two-dimensional vector. Fig. 3 shows the clustering result.

According to Fig. 3, it was found that the distribution of each subset is relatively concentrated, and there is a clear boundary between them and other subsets. The percentages of highly and weakly active inhibitors in the 12 subsets are shown in Fig. 4. And it was found that subsets 1, 3 and 6 have a large proportion of highly active inhibitors, while subsets 4 and 7 have a large proportion of weakly active inhibitors.

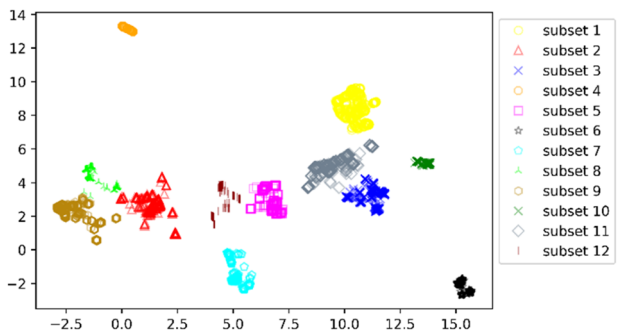

Fig. 3 Distribution of the 12 subsets.

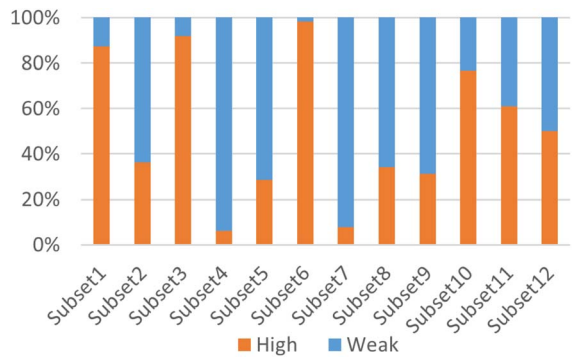

Fig. 4 The percentages of highly and weakly active inhibitors in the 12 subsets. High means the percentages of highly active inhibitors, represented by orange, and weak means the percentages of weakly active inhibitors, represented by blue.

Since dimension reduction will lead to the loss of molecular structure information of compounds, the use of UMAP two-dimensional vectors for clustering will cause the compounds in the same subset to maybe have different molecular scaffolds. We analysed the main scaffolds with a high number of compounds in each subset, and analysed fragment features of inhibitors containing these scaffolds by using statistical methods. Table 9 shows the scaffolds and fragment features on each subset.

According to Table 9, it was found that the compounds in subsets 1, 3, 7, 10, and 11 are 2-aminopyrimidine derivatives. The main scaffold of subset 1 is 9*H*-pyrido[4′,3′:4,5]pyrrolo[2,3-*d*]pyrimidin-2-amine, there were 425 highly active inhibitors and 65 weakly active inhibitors, and it was found that cyclopentane was more likely to appear in highly active inhibitors, while the hydroxyl group was more likely to appear in weakly active inhibitors. The main scaffold of subset 3 is 2-amino-*N*,*N*-dimethyl-7*H*-pyrrolo[2,3-*d*]pyrimidine-6-carboxamide, ribociclib[7] has this scaffold, there were 295 highly active inhibitors and 16 weakly active inhibitors, and it was found that cyclopentane, pyridine and piperazine were the most frequent fragments in the highly active inhibitors. The main scaffold of subset 7 is 9-(prop-2-yl)purin-2-amine, there were 21 highly active inhibitors and 224 weakly active inhibitors, and it was found that butane and cyclohexanamine were the most frequent fragments in the weakly active inhibitors. The main scaffold of subset 10 is 6,7,8,9-tetrahydropyrazino[2′,1′:5,1]pyrrolo[2,3-*d*]pyrimidin-2-amine, trilaciclib[9] has this scaffold, there were 84 highly active inhibitors and 2 weakly active inhibitors, and it was found that pyridine, piperazine and 7′,8′-dihydro-6′*H*-spiro[cyclohexane-1,9′-pyrazino[2′,1′:5,1]pyrrolo[2,3-*d*]pyrimidine]-6′-one were the most frequent fragments in the highly active inhibitors. The main scaffold of subset 11 is 2-amino-7,8-dihydropyrido[2,3-*d*]pyrimidin-7-one, palbociclib[6] has this scaffold, there were 99 highly active inhibitors and 61 weakly active inhibitors, and it was found that cyclopentane and piperazine were more likely to appear in highly active inhibitors, while benzene was more likely to appear in weakly active inhibitors.

The compounds in subsets 2, 4, and 6 are pyrazol derivatives. The compounds in subset 2 contain three main scaffolds, the first one is 2,4-dihydroindeno[1,2-*c*]pyrazol-4-one, there were 82 highly active inhibitors and 75 weakly active inhibitors, and it was found that 2-methyldiazane-1-carbaldehyde, the hydroxyl group, 1,4-oxazinane and thiophene were more likely to appear in highly active inhibitors, while isobutane was more likely to appear in weakly active inhibitors; the second one is quinazoline, there were 44 weakly active inhibitors, and it was found that fluoroform and isobutane were the most frequent fragments in the weakly active inhibitors; the third one is 1*H*-indazole, there were 5 highly active inhibitors and 25 weakly active inhibitors, and it was found that ethanol, phenol and methylbenzene were more likely to appear in highly active inhibitors, while formic acid, $1\lambda^6$-1,2-thiazolidine-1,1-dione and methanethiol were more likely to appear in weakly active inhibitors. The main scaffold of subset 4 is 4,5-dihydro-1*H*-

Table 9 Scaffolds and fragment features on the 12 subsets

Subset (high/weak)	Main scaffolds (high/weak)	Fragment			
		Structure	p_High[a]	p_Weak[a]	Diff[b]
Subset 1 (469/68)	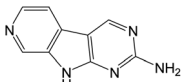 (425/65)		0.66	0.34	0.32
			0.41	0.65	−0.24
			0.20	0.40	−0.20
			0.44	0.05	0.39
	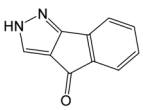 (82/75)		0.84	0.47	0.37
			0.35	0.03	0.33
			0.38	0.11	0.27
			0.07	0.23	0.15
Subset 2 (121/214)	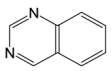 (0/44)		—	0.73	—
			—	0.73	—
			0.60	0.12	0.48
			0.60	0.16	0.44
	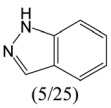 (5/25)		0.40	0.04	0.36
			0.00	0.84	−0.84
			0.00	0.84	−0.84
			0.00	0.84	−0.84
Subset 3 (311/28)	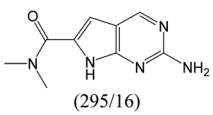 (295/16)		0.82	—	—
			0.77	—	—
			0.47	—	—
Subset 4 (6/93)	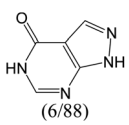 (6/88)		—	0.95	—
		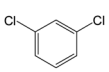	—	0.78	—

Table 9 (*Contd.*)

Subset (high/weak)	Main scaffolds (high/weak)	Fragment Structure	p_High[a]	p_Weak[a]	Diff[b]
Subset 5 (64/160)	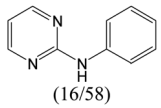 (16/58)		0.75	0.47	0.28
			0.56	0.36	0.20
			0.25	0.10	0.15
			0.00	0.12	−0.12
		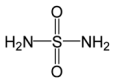	0.63	0.06	0.57
	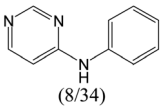 (8/34)		0.38	0.03	0.35
			0.25	0.09	0.16
			0.00	0.32	−0.32
			0.38	0.62	−0.24
	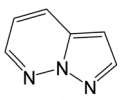 (28/30)		0.86	0.63	0.22
			0.21	0.03	0.18
			0.25	0.53	−0.28
		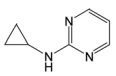	0.11	0.33	−0.23
		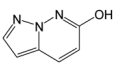	0.11	0.30	−0.19
Subset 6 (153/3)	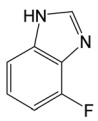 (126/3)		0.89	—	—
		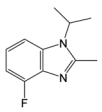	0.87	—	—
			0.82	—	—
Subset 7 (21/249)	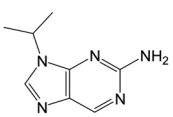 (21/224)		—	0.95	—
			—	0.71	—

Table 9 (*Contd.*)

Subset (high/weak)	Main scaffolds (high/weak)	Fragment Structure	p_High[a]	p_Weak[a]	Diff[b]
Subset 8 (52/101)	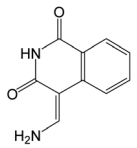 (44/55)		0.55	0.22	0.33
			0.34	0.07	0.27
			0.32	0.13	0.19
			0.14	0.40	−0.26
			0.16	0.35	−0.19
			1.00	0.48	0.52
	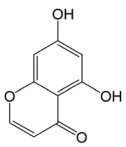 (5/25)		1.00	0.48	0.52
			0.60	0.28	0.32
		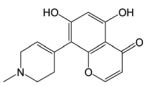	0.00	0.40	−0.40
		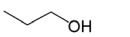	0.35	0.14	0.21
	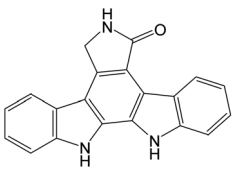 (40/21)	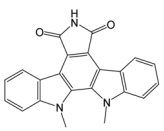	0.00	0.19	−0.19
		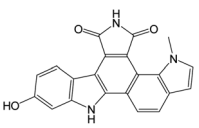	0.27	0.00	0.27
Subset 9 (112/247)	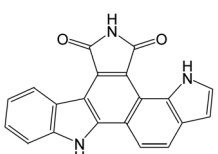 (63/8)	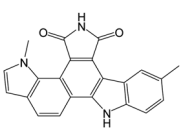	0.00	0.25	−0.25
		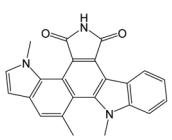	0.02	0.25	−0.23
	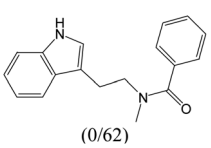 (0/62)	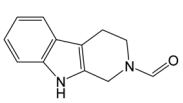	—	0.63	—
Subset 10 (86/26)	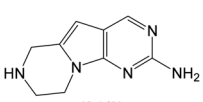 (84/2)		0.88	—	—
			0.80	—	—
		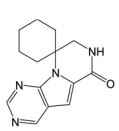	0.63	—	—

Table 9 (*Contd.*)

Subset (high/weak)	Main scaffolds (high/weak)	Fragment Structure	p_High[a]	p_Weak[a]	Diff[b]
Subset 11 (168/108)	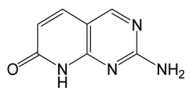 (99/61)		0.82	0.31	0.51
			0.64	0.21	0.42
			0.58	0.69	−0.11
	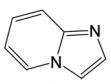 (0/30)	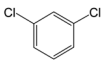	—	0.57	—
			—	0.57	—
		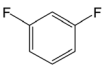	—	0.5	—
Subset 12 (79/79)	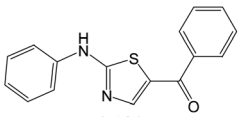 (58/1)		0.98	—	—
			0.34	—	—
			0.57	0.09	0.48
	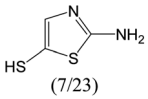 (7/23)		1.00	0.70	0.30
			1.00	0.78	0.22
			0.29	0.96	−0.67
			0.29	0.78	−0.50

[a] p_High and p_Weak are the frequency of the fragment in highly and weakly active inhibitors, respectively. [b] Diff, difference between p_High and p_Weak.

pyrazolo[3,4-*d*]pyrimidin-4-one, there were 6 highly active inhibitors and 88 weakly active inhibitors, and it was found that 1,3-dichlorobenzene and benzene were the most frequent fragments in the weakly active inhibitors. The main scaffold of subset 6 is 4-fluoro-1*H*-benzo[*d*]imidazole, abemaciclib[8] has this scaffold, there were 126 highly active inhibitors and 3 weakly active inhibitors, and it was found that pyridine, 5-fluoropyrimidine and 4-fluoro-2-methyl-1-(prop-2-yl)benzo[*d*]imidazole were the most frequent fragments in the highly active inhibitors.

The compounds in subset 5 contain three main scaffolds, the first one is 2-(phenylamino)pyrimidine, there were 16 highly active inhibitors and 58 weakly active inhibitors, and it was found that propane, phenol and 2-methyl-1-(prop-2-yl)imidazole were more likely to appear in highly active inhibitors, while 3-methyl-3*H*,2*H*-1,3-thiazol-2-one was more likely to appear in weakly active inhibitors; the second one is 4-(phenylamino)pyrimidine, there were 8 highly active inhibitors and 34 weakly active inhibitors, and it was found that azanesulfonamide, acetonitrile and piperazine were more likely to appear in highly active inhibitors, while methanesulfonamide and propan-2-ol were more likely to appear in weakly active inhibitors; the third one is pyrazolo[5,1-*f*][1,2]diazine, there were 28 highly active inhibitors and 30 weakly active inhibitors, and it was found that benzene and piperazine were more likely to appear in highly active inhibitors, while propane, 2-(cyclopropylamino)pyrimidine and pyrazolo[5,1-*f*][1,2]diazin-6-ol were more likely to appear in weakly active inhibitors.

The compounds in subset 8 contain two main scaffolds, the first one is 4-[(*Z*)-aminomethylidene]-1,2,3,4-tetrahydroisoquinoline-1,3-dione, there were 44 highly active inhibitors and 55 weakly active inhibitors, and it was found that phenol, pyridine and benzene-1,2-diol were more likely to appear in highly active inhibitors, while piperazine and hexahydropyridine were more likely to appear in weakly active inhibitors; the second one is 5,7-dihydroxy-4*H*-chromen-4-one, there were 5 highly active inhibitors and 25 weakly active inhibitors, and it was found that isobutane, chlorobenzene and 1-methylhexahydropyridin-3-ol were more likely to appear in highly active inhibitors, while 5,7-dihydroxy-8-(1-methyl-1,2,3,6-tetrahydropyridin-4-yl)-4*H*-chromen-4-one was more likely to appear in weakly active inhibitors.

The compounds in subset 9 contain three main scaffolds, the first one is 6,7,12,13-tetrahydro-5*H*-pyrrolo[4,3-*c*]indolo[2,3-*a*]carbazol-5-one, there were 40 highly active inhibitors and 21 weakly active inhibitors, and it was found that propan-1-ol was more likely to appear in highly active inhibitors, while 12,13-dimethyl-6*H*-pyrrolo[4,3-*c*]indolo[2,3-*a*]carbazole-5,7-dione was more likely to appear in weakly active inhibitors; the second one is 5,11-dihydro-3*H*-pyrrolo[4,3-*c*]indolo[6,7-*a*]carbazole-4,6-dione, there were 63 highly active inhibitors and 8 weakly active inhibitors, and it was found that 9-hydroxy-3-methyl-5,11-dihydropyrrolo[4,3-*c*]indolo[6,7-*a*]carbazole-4,6-dione was more likely to appear in highly active inhibitors, while 3,8-dimethyl-5,11-dihydropyrrolo[4,3-*c*]indolo[6,7-*a*]carbazole-4,6-dione was more likely to appear in weakly active inhibitors; the third one is *N*-[2-(1*H*-indol-3-yl)ethyl]-*N*-methylbenzamide, there were 62 weakly active inhibitors, and it was found that 2,3,4,9-tetrahydro-1*H*-pyrido[3,4-*b*]indole-2-carbaldehyde was the most frequent fragment in the weakly active inhibitors.

The compounds in subset 12 contain three main scaffolds, the first one is imidazo[1,2-*a*]pyridine, there were 30 weakly active inhibitors, and it was found that 1,3-dichlorobenzene, dimethylamine and 1,3-difluorobenzene were the most frequent fragments in the weakly active inhibitors; the second one is phenyl[2-(phenylamino)-1,3-thiazol-5-yl]methanone, there were 58 highly active inhibitors and 1 weakly active inhibitor, and it was found that methanol and fluorobenzene were the most frequent fragments in the highly active inhibitors; the third one is 2-amino-1,3-thiazole-5-thiol, there were 7 highly active inhibitors and 23 weakly active inhibitors, and it was found that pyridine and isobutane were more likely to appear in highly active inhibitors, while formaldehyde and formic acid were more likely to appear in weakly active inhibitors.

In summary, it was found that piperazine, cyclopentane, pyridine and 2-aminopyrimidine were common fragments in highly active inhibitors.

Conclusion

In this study, we collected 3018 CDK4 inhibitors and their IC_{50} values. Two training sets and test sets were divided by SOM and random method. MACCS fingerprints, ECFP4 fingerprints and Corina descriptors were calculated and extracted. 18 classification models were built by inputting three types of descriptors and using Random Forest, Support Vector Machine and Deep Neural Network methods. Model A2 and Model B5 are the optimal models based on the two different training sets. The prediction accuracy of Model A2 on the test set is 93.88% and MCC is 0.874. The prediction accuracy of Model B5 on the test set is 89.93% and MCC is 0.798. The application domain of the 18 classification models was calculated, and the performances of the models in the application domain were recalculated, and it was found that the performances had improved in the application domain.

We considered adding decoys to train models and evaluate their performance, because decoys are necessary to evaluate virtual screening methods. Therefore, we used two different decoy generation methods in training and test sets, respectively. Then, MACCS fingerprints, ECFP4 fingerprints and Corina descriptors were calculated and extracted. The 18 classification models were built by inputting three types of descriptors and using Random Forest, Support Vector Machine and Deep Neural Network methods. Model C2 and Model D5 are the optimal models based on the two different training sets. The prediction accuracy of Model C2 on the test set is 98.5% and MCC is 0.937. The prediction accuracy of Model D5 on the test set is 87.32% and MCC is 0.881. Compared to the other 18 classification models (Models A1–A9 and B1–B9 in Table 2), it was found that the more samples used for modelling, the more robust the models, and the better the performance of the models.

On the basis of 3018 CDK4 inhibitors, we selected 1427 CDK4 inhibitors whose IC_{50} was detected by a radiolabeling method to build QSAR models. Two training sets and test sets were divided by SOM and random method. Corina, MOE and RDkit descriptors of the compounds were calculated and extracted, and 24 QSAR models were built by inputting three types of descriptors and using Multiple Linear Regression, Random Forest, Support Vector Machine and Deep Neural Network methods. Model E3 and Model F7 are the optimal models based on the two different training sets. The prediction R^2 of Model E3 on the test set is 0.805 and RMSE is 0.561. The prediction R^2 of Model F7 on the test set is 0.824 and RMSE is 0.534. The application domain of Model E3 and Model F7 was calculated, and the performances of the models in the application domain were recalculated, and it was found that the RMSE predicted on the test set had improved in the application domain, indicating that some outliers with large prediction deviation could be deleted in the application domain, and the compound prediction in the application domain was considered to be reliable.

In addition, we used UMAP and *K*-means to cluster 3018 inhibitors into 12 subsets and analysed the scaffolds and fragment features of CDK4 inhibitors. It was found that piperazine, cyclopentane, 2-aminopyrimidine and pyridine were important structures in the highly active inhibitors.

Data availability

All the data (dataset) used for modelling and all of the code of this study are provided at **https://github.com/pangxiaoyang/qsar/tree/master**.

Author contributions

Xiaoyang Pang built the models and analysed the structural features. Yunyang Zhao and Guo Li performed the analysis of the results of the models. Jianrong Liu and Aixia Yan provided the main idea of this work. All authors read and approved the final manuscript.

Conflicts of interest

There are no conflicts to declare.

Acknowledgements

We thank Molecular Networks GmbH, Nuremberg, Germany, for providing the programs CORINA Symphony and SONNIA for our scientific work.

References

1 T. Adon, D. Shanmugarajan and H. Y. Kumar, *RSC Adv.*, 2021, **11**, 29227–29246.
2 R. Wang, K. Xu, F. Gao, J. Huang and X. Guan, *Biochim. Biophys. Acta, Rev. Cancer*, 2021, **1876**, 188590.
3 V. Wagner and J. Gil, *Oncogene*, 2020, **39**, 5165–5176.
4 A. Fassl, Y. Geng and P. Sicinski, *Science*, 2022, **375**, eabc1495.
5 C. L. Braal, E. M. Jongbloed, S. M. Wilting, R. H. J. Mathijssen, S. L. W. Koolen and A. Jager, *Drugs*, 2021, **81**, 317–331.
6 P. L. Toogood, P. J. Harvey, J. T. Repine, D. J. Sheehan, S. N. VanderWel, H. Zhou, P. R. Keller, D. J. McNamara, D. Sherry, T. Zhu, J. Brodfuehrer, C. Choi, M. R. Barvian and D. W. Fry, *J. Med. Chem.*, 2005, **48**, 2388–2406.
7 U. Asghar, A. K. Witkiewicz, N. C. Turner and E. S. Knudsen, *Nat. Rev. Drug Discovery*, 2015, **14**, 130–146.
8 C. Zha, W. Deng, Y. Fu, S. Tang, X. Lan, Y. Ye, Y. Su, L. Jiang, Y. Chen, Y. Huang, J. Ding, M. Geng, M. Huang and H. Wan, *Eur. J. Med. Chem.*, 2018, **148**, 140–153.
9 C. Sánchez-Martínez, M. J. Lallena, S. G. Sanfeliciano and A. de Dios, *Bioorg. Med. Chem. Lett.*, 2019, **29**, 126637.
10 X. Li, P. Sun, J. Lan, J. Peng, Y. Chen, B. Wang and Q. Dong, WO Patent, WO2014183520A1, 2014.
11 F. R. Wilson, A. Varu, D. Mitra, C. Cameron and S. Iyer, *Breast Cancer Res. Treat.*, 2017, **166**, 167–177.
12 G. N. Hortobagyi, S. M. Stemmer, H. A. Burris, Y. S. Yap, G. S. Sonke, S. Paluch-Shimon, M. Campone, K. L. Blackwell, F. Andre, E. P. Winer, W. Janni, S. Verma, P. Conte, C. L. Arteaga, D. A. Cameron, K. Petrakova, L. L. Hart, C. Villanueva, A. Chan, E. Jakobsen, A. Nusch, O. Burdaeva, E. M. Grischke, E. Alba, E. Wist, N. Marschner, A. M. Favret, D. Yardley, T. Bachelot, L. M. Tseng, S. Blau, F. Xuan, F. Souami, M. Miller, C. Germa, S. Hirawat and J. O'Shaughnessy, *N. Engl. J. Med.*, 2016, **375**, 1738–1748.
13 M. N. Dickler, S. M. Tolaney, H. S. Rugo, J. Cortes, V. Dieras, D. Patt, H. Wildiers, C. A. Hudis, J. O'Shaughnessy, E. Zamora, D. A. Yardley, M. Frenzel, A. Koustenis and J. Baselga, *Clin. Cancer Res.*, 2017, **23**, 5218–5224.
14 M. P. Goetz, M. Toi, M. Campone, J. Sohn, S. Paluch-Shimon, J. Huober, I. H. Park, O. Trédan, S. C. Chen, L. Manso, O. C. Freedman, G. Garnica Jaliffe, T. Forrester, M. Frenzel, S. Barriga, I. C. Smith, N. Bourayou and A. Di Leo, *J. Clin. Oncol.*, 2017, **35**, 3638–3646.
15 G. W. Sledge Jr, M. Toi, P. Neven, J. Sohn, K. Inoue, X. Pivot, O. Burdaeva, M. Okera, N. Masuda, P. A. Kaufman, H. Koh, E. M. Grischke, M. Frenzel, Y. Lin, S. Barriga, I. C. Smith, N. Bourayou and A. Llombart-Cussac, *J. Clin. Oncol.*, 2017, **35**, 2875–2884.
16 A. Y. Lai, J. A. Sorrentino, K. H. Dragnev, J. M. Weiss, T. K. Owonikoko, J. A. Rytlewski, J. Hood, Z. Yang, R. K. Malik, J. C. Strum and P. J. Roberts, *Immunother. Cancer*, 2020, **8**, e000847.
17 N. Portman, S. Alexandrou, E. Carson, S. Wang, E. Lim and C. E. Caldon, *Endocr.-Relat. Cancer*, 2019, **26**, R15–R30.
18 J. L. F. Teh and A. E. Aplin, *Clin. Cancer Res.*, 2019, **25**, 921–927.
19 K. Pandey, H. J. An, S. K. Kim, S. A. Lee, S. Kim, S. M. Lim, G. M. Kim, J. Sohn and Y. W. Moon, *Int. J. Cancer*, 2019, **145**, 1179–1188.
20 M. Álvarez-Fernández and M. Malumbres, *Cancer Cell*, 2020, **37**, 514–529.
21 V. T. Sabe, T. Ntombela, L. A. Jhamba, G. E. M. Maguire, T. Govender, T. Naicker and H. G. Kruger, *Eur. J. Med. Chem.*, 2021, **224**, 113705.
22 Y. Wu, D. Huo, G. Chen and A. Yan, *SAR QSAR Environ. Res.*, 2021, **32**, 85–110.
23 Z. Zhang, Y. Tian and A. Yan, *CCF Trans. High Perform. Comput.*, 2021, **3**, 353–364.
24 R. Qin, H. Wang and A. Yan, *SAR QSAR Environ. Res.*, 2021, **32**, 411–431.
25 D. Qu, A. Yan and J. S. Zhang, *SAR QSAR Environ. Res.*, 2017, **28**, 111–132.
26 D. Huo, S. Wang, Y. Kong, Z. Qin and A. Yan, *J. Chem. Inf. Model.*, 2021, 5149–5164, DOI: **10.1021/acs.jcim.1c00884**.
27 M. N. Gomes, R. C. Braga, E. M. Grzelak, B. J. Neves, E. Muratov, R. Ma, L. L. Klein, S. Cho, G. R. Oliveira, S. G. Franzblau and C. H. Andrade, *Eur. J. Med. Chem.*, 2017, **137**, 126–138.
28 B.-q. Cai, H.-x. Jin, X.-j. Yan, P. Zhu and G.-x. Hu, *Acta Pharmacol. Sin.*, 2014, **35**, 151–160.
29 N. Dessalew and P. V. Bharatam, *Eur. J. Med. Chem.*, 2007, **42**, 1014–1027.
30 V. Divya, V. L. Pushpa and K. B. Manoj, *J. Mol. Struct.*, 2019, **1183**, 263–273.
31 M. Gupta and A. K. Madan, *J. Chem. Sci.*, 2013, **125**, 483–493.
32 X.-Y. Lu, Y.-D. Chen, N.-y. Sun, Y.-J. Jiang and Q.-D. You, *J. Mol. Model.*, 2010, **16**, 163–173.
33 H. Lv, Y. Du, X. Sheng, Z. Gao and J. Shen, *Future Med. Chem.*, 2021, **13**, 1317–1339.
34 M. Muzaffar-ur-Rehman, S. K. Gunda, L. Corrie and B. P. Kumar, *Indo Am. J. Pharm. Sci.*, 2017, **4**, 2981–2993.
35 A. Pandrangi, *J. Pharm. Innov.*, 2014, **3**, 164–169.
36 R. Rondla, L. S. Padma Rao, V. Ramatenki, R. Vadija, T. Mukkera, S. R. Potlapally and U. Vuruputuri, *J. Mol. Struct.*, 2017, **1134**, 482–491.
37 A. Sharma and N. Agarwal, *Pharm. Chem. J.*, 2021, **13**, 26–43.
38 M. O. Sarhan, S. S. Abd El-Karim, M. M. Anwar, R. H. Gouda, W. A. Zaghary and M. A. Khedr, *Molecules*, 2021, **26**, 2273.
39 A.-A. Omar Husham Ahmed and M. Mohd Nizam, *J. Appl. Pharm. Sci.*, 2022, 165–175, DOI: **10.7324/japs.2021.120116**.
40 F. Le, L.-N. Zhao, H.-M. Guo, Y. Na, W.-X. Quan, C. Yi, S. Mao, W. Rui and Z.-H. Lin, *Chin. J. Struct. Chem.*, 2022, **41**, 2203108–2203124.
41 S. Misra, H. Li and J. He, in *Machine Learning for Subsurface Characterization*, ed. S. Misra, H. Li and J. He, Gulf

Professional Publishing, 2020, pp. 129–155, DOI: 10.1016/B978-0-12-817736-5.00005-3.
42 SONNIA, *Version 4.2; MolecularNetworksGmbH: Erlangen, Germany.[EB/OL]*, 2020.03.12, http://www.molecular-networks.com.
43 Y. O. Adeshina, E. J. Deeds and J. Karanicolas, *Proc. Natl. Acad. Sci. U. S. A.*, 2020, **117**, 18477–18488.
44 P. J. Ballester, *Drug Discovery Today: Technol.*, 2019, **32–33**, 81–87.
45 F. Imrie, A. R. Bradley and C. M. Deane, *Bioinformatics*, 2021, **37**, 2134–2141.
46 J. Xia, S. Li, Y. Ding, S. Wu and X. S. Wang, *Mol. Inf.*, 2020, **39**, e1900151.
47 P. Carracedo-Reboredo, J. Liñares-Blanco, N. Rodríguez-Fernández, F. Cedrón, F. J. Novoa, A. Carballal, V. Maojo, A. Pazos and C. Fernandez-Lozano, *Comput. Struct. Biotechnol. J.*, 2021, **19**, 4538–4558.
48 D. Rogers and M. Hahn, *J. Chem. Inf. Model.*, 2010, **50**, 742–754.
49 *DrugBank Release Version 5.1.3 – DrugBank[EB/OL]*, 2020.03.12, www.molecularnetworks.com.
50 G. Landrum, *Rdkit: Open-source cheminformatics software[EB/OL]. 2020.09.1*, http://www.rdkit.org/.
51 D. Nettleton, in *Commercial Data Mining*, ed. D. Nettleton, Morgan Kaufmann, Boston, 2014, pp. 79–104, DOI: DOI: 10.1016/B978-0-12-416602-8.00006-6.
52 Chemical Computing Group Inc., *Molecular Operating Environment (MOE)*, Montreal, QC, Canada, 2016.
53 L. Breiman, *Mach. Learn.*, 2001, **45**, 5–32.
54 C. Cortes and V. Vapnik, *Mach. Learn.*, 1995, **20**, 273–297.
55 Y. Xu, J. Ma, A. Liaw, R. P. Sheridan and V. Svetnik, *J. Chem. Inf. Model.*, 2017, **57**, 2490–2504.
56 F. Pedregosa, G. Varoquaux, A. Gramfort, V. Michel, B. Thirion, O. Grisel, M. Blondel, P. Prettenhofer, R. Weiss, V. Dubourg, J. Vanderplas, A. Passos, D. Cournapeau, M. Brucher, M. Perrot and É. Duchesnay, *J. Mach. Learn. Res.*, 2011, **12**, 2825–2830.
57 M. Mete, U. Sakoglu, J. S. Spence, M. D. Devous, T. S. Harris and B. Adinoff, *BMC Bioinf.*, 2016, **17**, 357.
58 Y. Jung and J. Hu, *J. Nonparametric Stat.*, 2015, **27**, 167–179.
59 D. Krstajic, L. J. Buturovic, D. E. Leahy and S. Thomas, *J. Cheminf.*, 2014, **6**, 10.
60 S. Ioffe, C. Szegedy, *International Conference on Machine Learning*, 2015, vol. 37, pp. 448–456.
61 D. P. Kingma and J. Ba, *Computer Science*, 2014, 1–15.
62 L. Prechelt, *Neural Networks*, 1998, **11**, 761–767.
63 A. Paszke, S. Gross, F. Massa, A. Lerer, J. Bradbury, G. Chanan, T. Killeen, Z. Lin, N. Gimelshein, L. Antiga, A. Desmaison, A. Köpf, E. Yang, Z. DeVito, M. Raison, A. Tejani, S. Chilamkurthy, B. Steiner, L. Fang and S. Chintala, *PyTorch: An Imperative Style, High-Performance Deep Learning Library*, 2019.
64 D. J. Livingstone and D. W. Salt, *J. Med. Chem.*, 2005, **48**, 661–663.
65 M. Baltruschat and P. Czodrowski, *F1000Research*, 2020, **9**, 1–16.
66 R. Parikh, A. Mathai, S. Parikh, G. Chandra Sekhar and R. Thomas, *Indian J. Ophthalmol.*, 2008, **56**, 45–50.
67 D. Chicco, N. Tötsch and G. Jurman, *BioData Min.*, 2021, **14**, 13.
68 S. Vad, A. Eskinazi, T. Corbett, T. McGloughlin and J. P. Vande Geest, *J. Biomech. Eng.*, 2010, **132**, 121007.
69 I. Sushko, S. Novotarskyi, R. Körner, A. K. Pandey, A. Cherkasov, J. Li, P. Gramatica, K. Hansen, T. Schroeter, K.-R. Müller, L. Xi, H. Liu, X. Yao, T. Öberg, F. Hormozdiari, P. Dao, C. Sahinalp, R. Todeschini, P. Polishchuk, A. Artemenko, V. Kuz'min, T. M. Martin, D. M. Young, D. Fourches, E. Muratov, A. Tropsha, I. Baskin, D. Horvath, G. Marcou, C. Muller, A. Varnek, V. V. Prokopenko and I. V. Tetko, *J. Chem. Inf. Model.*, 2010, **50**, 2094–2111.
70 P. Gramatica, *QSAR Comb. Sci.*, 2007, **26**, 694–701.
71 F. Camastra and A. Verri, *IEEE Trans. Pattern Anal. Mach. Intell.*, 2005, **27**, 801–805.
72 S. Hernández-Hernández and P. J. Ballester, *Biomolecules*, 2023, **13**, 1–19.
73 V. D. M. Laurens and G. Hinton, *J. Mach. Learn. Res.*, 2008, **9**, 2579–2605.